WILEY-VCH

Porous Bilayer Electrode Guided Gas Diffusion for Enhanced CO_2 Electrochemical Reduction

Yucheng Wang, Hanhui Lei, Hang Xiang, Yongqing Fu, Chenxi Xu, Yinzhu Jiang, Ben Bin Xu, Eileen Hao Yu*, Chao Gao*, Terence Xiaoteng Liu**

Y. Wang, H. Lei, Prof. Y. Fu, Prof. B.B. Xu, Dr. T.X. Liu
Faculty of Engineering and Environment, Northumbria University, Newcastle upon Tyne, NE1 8ST, United Kingdom
E-mail: ben.xu@northumbria.ac.uk, terence.liu@northumbria.ac.uk

H. Xiang, Prof. C. Xu, Prof. E.H. Yu
School of Engineering, Newcastle University, Newcastle Upon Tyne, NE1 7RU, United Kingdom

Prof. C. Xu
Department of Materials Science and Engineering, Hefei University of Technology, Hefei, 230009, P. R. China

Prof. Y. Jiang
School of Materials Science and Engineering, State Key Laboratory of Clean Energy Utilization, Zhejiang University, Hangzhou, 310027, P. R. China

Prof. E.H. Yu
Department of Chemical Engineering, Loughborough University, Loughborough, LE11 3TU, United Kingdom
E-mail: E.Yu@lboro.ac.uk

Prof. C. Gao
MOE Key Laboratory of Macromolecular Synthesis and Functionalization, Department of Polymer Science and Engineering, Key Laboratory of Adsorption and Separation Materials & Technologies of Zhejiang Province, Zhejiang University, 38 Zheda Road, Hangzhou, 310027, P. R. China
E-mail: chaogao@zju.edu.cn

Keywords: CO_2 reduction reaction, gas diffusion electrode, mass transfer, graphene aerogel.

Abstract

Comparing to the massive efforts in developing innovative catalyst materials system and technologies, structural design of cells has attracted less attentions on the road towards high performance electrochemical CO_2 reduction reaction (eCO_2RR). Here, we propose a hybrid gas diffusion electrode-based reaction cell by using highly porous carbon paper (CP) and graphene aerogels (GA), which is expected to offer directional diffusion of gas molecules onto the catalyst bed, to sustain a high performance in CO_2 conversion. The above hypothesis has been supported by the experimental and simulation results, which show that the CP + GA combined configuration increases the Faraday efficiency (FE) from ~ 60% to over 94% towards carbon monoxide (CO) and formate production compared with a CP only cell with Cu_2O as the catalyst. It also suppresses the undesirable side reaction - hydrogen evolution over 65 times than the conventional H-type cell (H-cell). By combining with advanced catalysts with high selectivity, a 100% FE of the cell with a high current density could be realised. The described strategy sheds an extra light on future development of eCO_2RR with a structural design of cell enabled high CO_2 conversion.

Carbon dioxide (CO_2) capture and utilisation have been frequently described as promising technical routes in the numerous decarbonization manifestos in the last few decades, with the advantages of producing high value chemical products and energy feedstock[1]. Among all technologies envisaged by far, electrochemical reduction of CO_2 has been recognised as a distinguished candidate on the road toward highly efficient conversion of CO_2 at scale-up applications, because of its controllable process[2], moderate reactions under ambient conditions[3, 4], and highly designable and productive outputs (e.g. CO, CH_4, C_2H_2, C_2H_4, formic acid (HCOOH), methanol (CH_3OH), and ethanol (CH_3CH_2OH))[5]. However, a number of challenges in the eCO_2RR remain to be tackled, e.g., inertness of CO_2[6] which requires a high overpotential to be kinetically activated, its low solubility in electrolyte[7] that easily lead to low efficient reaction, desired yield selection process for mixed productions through enhance selectivity[8] and catalytic activity[9], and durability of the reaction/system[10, 11] especially at a scale-up process.

Current researches in eCO_2RR mostly focus on developing novel catalysts with designed morphology[12], crystallization[13] and particle size[14], in order to realise an enhanced selectivity and FE for a desired eCO_2RR process/product. The eCO_2RR is usually taken place within a conventional H-cell [15, 16] consisting of a working electrode made by porous materials, e.g. carbon paper[17] and metal mesh[18]. Recent advancement in electrode design has achieved gas diffusion electrode (GDE) to enhance the mass transfer in eCO_2RR, where the gas diffusion in porous media lead to the retention of CO_2 within the electrode to extend the saturation on the catalyst bed. Therefore, a desired mass transfer of CO_2 can be facilitated to limit hydrogen evolution and improve reaction rate of eCO_2RR for a higher FE and selectivity. Xiang *et al*. reported a porous conductive CP based GDE to achieve more than 5-fold in efficiency (current density) of that from the conventional H-cell[19, 20]. Further developments provided perspectives to optimise the mass

transfer for high conversion rate of eCO_2RR by designing the surface/interface and geometrical features of electrodes[21], for example, García de Arquer et al.[22] developed a catalyst : ionomer bulk heterojunction GDE design to achieve higher CO_2 electrochemical reduction with an ethylene partial current density of 1.3 amperes per square centimeter at 45% cathodic energy efficiency.

Theoretical understanding on the mass transfer in porous media remain to be fully explored, since it could be influenced by many factors, e.g. catalyst, electrode material, electrolyte, electrode assembly as well as the molar concentration of the reactant gas along the electrocatalyst surfaces. However, it has been well-known that the gas diffusion in porous media can lead to the retention of CO_2 within the electrode to extend saturation on the catalysts, thus enhancing reaction kinetics, FE and selectivity.

Here, we introduce a porous hybrid bi-layer design with interface of two porous materials, aiming to create alternative mass transfer by establishing the circulation/diffusion sub-cycle for an improved eCO_2RR performance. We firstly design and compare four types of electrochemical reactors (**Figure S1**), with the first design is a compact H-cell (Figure S1a and **Figure S5**a). Comparing with the conventional H-cell[16], this compact H-cell presents incremental optimization by offering more areas for the working electrode but less spaces between cathode and anode (ca. 1 cm). This can result into a lower electrolyte resistance (causing an overpotential) for electro-chemical behaviour[23]. This type of gas supply will inevitably enable poor CO_2 transfer caused by the low solubility of CO_2 in electrolyte[24], while hydrogen evolution reaction (HER) will also happen and reduce the CO_2 reduction efficiency[25, 26]. Meanwhile, CO_2 supplying method based on the idea of 'bubbling into electrolyte' will be likely to occur to destabilize the system, where some CO_2 bubbles will stick on the surface of working electrode and block the pathway of proton

transfer to the catalyst surface (**Figure S2**). These will yield less electrode areas for reaction, thus leading to a significantly decrease in current density.

The core structure for the second design (CP-cell) is a conventional carbon paper (CP) based GDE which serves as a current collector and foundation to support the catalyst layer (**Figure 1**a). The integrated CP-cell design is illustrated in Figure 1c and Figure S1b, where the catalyst layer with an average thickness of 10 μm is homogenously attached on the CP surface (Figure 1e). However, the carbon paper will degrade after a long-term reaction, and the permeation of water easily occur in this type of cell to trigger HER as well as the blockage of CO_2 mass transfer pathway. Additionally, an inhomogeneous CO_2 gas flow is often observed in carbon paper base GDE design due to some of above reasons.

Graphene aerogel (GA) has been considered as a promising electrode material for different scenarios, particularly for its bespoken porosity and stability etc. Our group previously developed a direct methanol fuel cell (DMFC) technology with an enhanced mass power density by replacing carbon paper with GA[27]. The concept of GA GDE is introduced in the 3rd design (**Figure S4**a) with an integrated cell design (GA-cell) shown in Figure S4b and Figure S1c, where the GA is inserted in the chamber to allow CO_2 to diffuse within the highly porous GA rather than passing through the empty chamber. The high porosity of GA offers a large surface area and a reasonably good conductivity ($\approx$10 S cm^{-1})[27], which make it a suitable material as a foundation to host catalyst. Moreover, the 3D structure of GA could resist the permeation of electrolyte effectively. It should be noted that, the high roughness on GA's surface could be problematic during the coating process for catalyst, even at a higher loading of 5 mg cm^{-2} or after surface treatment, thus leading to a coarse structure and exposing the GA to the electrolyte (Figure S4a and **Figure S6**c).

Next, we create a porous hybrid bi-layer design (GACP-cell) by practically combining GA (without catalyst, Figure 1e inset) to the CP GDE. A schematic of this bi-layer GDE configuration and an integrated cell design are shown in Figure 1b and Figure 1d, where GA fills the gas chamber with a very gentle pressure (~ 1 N/cm^2) applied from the CP to ensure an intimate contact, the current collector is attached to CP which is the same construction to the CP-cell for the purpose of maintain the same overall device resistance to avoid possible interruption to the charge transfer. Electrochemical impedance spectroscopy (EIS) is utilised to assess all GDE cells prior to the CO_2RR testing, the Nyquist plots (**Figure S7**) indicate that all cells display similar value of R_{ct}, suggesting there is ignorable charge transfer in the following CO_2RR testing for all GDE cells.

An interface effect is expected to increase the mass transfer of CO_2 with a guided diffusion on the catalyst layer (Figure 1f). We next utilised 3D printing technique to create the parts with the design details of GACP-cell (Figure 1g, Figure 1i and Figure S1d) and then fully assembly of the device (Figure 1j). The GACP-cell consists of three chambers. The gas chamber in the left-hand side contains GA, where the CO_2 flows into gas chamber, diffuses through GA and then CP, and finally reaches to the catalyst layer. The middle chamber is filled with catholyte, where the cathode coated with catalyst (Figure 1h) is exposed to the catholyte, and a reference electrode is inserted in this chamber. The right chamber is the anode chamber with anolyte and the inserted counter electrode (Pt wire). A cation exchange membrane is placed between the anode and cathode chambers to allow H^+ to pass through. All the components with gaskets are firmly connected and sealed to ensure a good contact without any leakage**.** The whole cell was designed to reduce the electrolyte resistance (more details can be found in SI, Experimental Methods).

Since the pore sizes in the carbon paper and graphene aerogel are larger than 10 μm, the CO_2 mass transfer in these two media can only be through gas flow. When CO_2 approaches to catalyst

layer, a gas concentration gradient is generated near the catalyst layer as result of gas diffusion, which can be predicted by the Fick's second law[28].

$$\frac{\partial C}{\partial t} = D_a \frac{\partial^2 C}{\partial x^2} \quad (1)$$

where C refers to the CO_2 molar concentration (mol/L^3), t is the time (s), D_a is the molecular diffusion coefficient in air ($L^2 \cdot s^{-1}$), and x is the distance along the axis of flow (L). Compared with the CP-cell, the GA cell shows a constant CO_2 flow before approaching to catalyst layer, which will increase CO_2 molar concentration with a homogenous distribution. The interface between the CP and GA layers plays a key role by acting as a boundary for the gas transfer, where the occurrence of sub-circulation is expected to enhance the CO_2 gas diffusion and prevent the water penetration.

To explore and compare the mass transfer for the cell designs, COMSOL® simulation of real time CO_2 molar concentrations along the cathode catalyst layer has been performed for the CP-cell, GA-cell and GACP-cell (**Figures 2** a-c). The simulations are set based on the following assumptions: 1. There is no thermal expansion; 2. Sufficient CO_2 is supplied from the inlet; 3. CO_2 is reacted immediately once arriving the catalyst layer; 4. The morphology of membrane is sustained throughout the reaction with no residual stress to cause the rupture; 5. Acid-base equilibria that occurs at the catalyst layer-electrolyte boundary is omitted. Detailed parameters, settings and conditions in the simulations are summarised in Tables S1 and S2.

The simulation outcomes show that the CO_2 molar concentration for CP-cell (Figure 2a), is generally lower than those from the other cells. The GA-cell (Figure 2b) appears to have a high CO_2 molar concentration around the inlet with a fast-decreasing gradient, and the rest of the electrode shows a nearly constant CO_2 molar concentration, which is slightly higher than that of

CP cell. The GA increases CO_2 gas diffusion within the electrode and reduce its transferring speed prior to leave the chamber for a higher reaction efficiency. The CO_2 molar concentration is effectively enhanced in the GACP-cell, because the CO_2 feedstock supplies reactant more evenly through its body to the catalyst layer. An explicit improvement in the uniformity of CO_2 molar concentrations is obtained (Figure 2c) along the electrode surface, in which a homogeneous distribution is observed. A higher FE value and a better eCO_2RR performance can be realised due to the improved mass transfer from the abundant supply of reactant.

The catalyst system used in this research are homemade Cu_2O and commercially available antimony tin oxide (ATO) nanoparticles. It has been reported that the Cu_2O has a high electrocatalytic activity to produce CO with a high value of FE under ambient conditions[10, 29], and antimony oxide and tin oxide are reported to have good activity on generating formate[30]. Therefore, ATO is used to assess high value of FE of formate for both gas and liquid productions. These catalysts were coated onto the surface of carbon paper with a loading of 5 mg cm^{-2}.

The FE results of CP-cell, GA-cell, GACP-cell and H-cell are shown in Figures 2d-2g (more information in Tables S3-S6), where the green bars represent H_2 generated from HER, yellow bars represent CO, and the blue bars represent formate. The total current density and current density of CO generated from Autolab® potentiostat are shown in Figure 2h and 2i (more information in Tables S7 and S8). It can be seen from Figure 2g that the HER dominates the reaction in the H-cell, with a small amount of CO and formate produced at -0.4 V *vs*. RHE. At low potentials, the main product is hydrogen as the overpotential of HER in the alkaline environment is near to 0 V vs. RHE. There is an increase of FE value for the CO when increasing potential, but that of the formate remains unchanged. For the H-cell, in the aqueous media, CO_2 gas is dissolved in catholyte and form CO_2(aq.), which is then transferred from the catholyte to surface of the catalyst layer[20].

This is known as acid-base equilibrium which could be another reason influences the eCO_2RR FE values. Meanwhile, a low solubility will limit CO_2 supply and thus the HER will happen when there is absence of CO_2, eventually lead to a low FE of carbonaceous products[25].

Increasing the solubility of CO_2 in electrolyte has been seen as one of the promising means to enhance CO_2 mass transfer in H-cell, in which CO_2 was supplied under high pressure and high temperature to address the solubility issues[20]. However, the non-ambient processing conditions may destabilise the system and are less feasible for scale-up application. A re-configuration of the CO_2-liquid-supplying is desirable for mass transfer problem from above perspectives. Although the above solutions may improve the mass transfer by enhancing the solubility of CO_2, it is theoretically relied upon CO_2 in liquid phase devices for eCO_2RR. Besides, K^+ in electrolyte would be easily bound onto the electrode and prohibit CO_2 diffusion[20, 31], which leads to the overall reaction turning into water splitting.

The CP-cell shows a much higher FE value of CO than that of H-cell as shown in Figure 2d. Its FE values of CO at potentials of -0.4 V, -0.6 V, -0.8 V, -1.0 V,-1.2 V, are 55.13%, 65.71%, 60.19%, 64.23%, 58.93%, and the FEs of formate at potentials of -0.4 V -0.6 V, -0.8 V, -1.0 V, -1.2 V, are 2.95%, 2.83%, 2.42%, 1.54%, and 2.19%, respectively. The decreased FE values towards HER are resulted from the minimised exposure of carbon paper and the creation of three phase boundaries which improve the CO_2 mass transfer. As shown in Figure 1e of the cross-sectional view of the CP GDE, the catalyst is formed a uniform layer with a thickness of 10 μm, and the CP was pre-treated with polytetrafluoroethylene (PTFE) layer to block the water. In this configuration, the CO_2 gas can directly reach to the catalyst layer, thus overcoming the gas diffusion limitations in the electrolyte.

Among these three new devices, the GA-cell presents the lowest FE value of formate as shown in Figure 2e. A large amount of graphene is exposed while printed with the catalyst ink, and this yields an inhomogeneous catalyst layer. Even with a high catalyst loading of 5 mg cm^{-2} (Figure S6c), there is still exposure of GA 'skeleton' (graphene) which takes part in HER. Moreover, the organic-friendly GA may absorb the formate and reduce its concentration, which can be detected in the ion chromatography (IC) test. The FE values of CO are 29.97%, 12.34%, 13.62%, 9.86%, 4.17% at potentials from -0.4 V to -1.2 V.

Once a plain GA was attached at the back of the CP GDE, the GACP-cell is constructed. In Figure 2f, the FE values of CO are enhanced to 79.58%, 80.41%, 84.20%, 83.54%, 81.91% and the FE values of formate are increased to 8.47%, 9.73%, 9.81%, 11.35%, 10.73%, respectively, at -0.4 V to -1.2 V potentials for the GACP-cell. This new cell suppressed the FE values of H_2 from HER to 11.95%, 9.86%, 5.99%, 5.11%, 7.36%, at -0.4 V to -1.2 V, which is a dramatic 11 times improvement compare to those of the H-cell. Compare with CP cell, GACP cell presents higher current density (Figure 2h) in the potential ranged from -0.4 V to -0.8 V vs. RHE, and the H-cell shows a higher current density at a larger negative potential. This shows the evidence that the HER is dominated the reaction. From the current density of the desired product CO (Figure 2i), it is obvious that the GACP-cell presents the highest current density for CO production. The above experimental results confirm our prospective that the improvement in mass transfer induces a higher CO_2 molar concentration, and it also agrees well with the simulation results.

COMSOL® simulation results of over-potential (OP) distribution along the cathode catalyst layers for CP-cell, GA-cell and GACP-cell are presented in **Figure S8**. All results show a mixed distribution of the OP ranges from -0.2 V to 0 V. The HER occurs at OP near to 0 V. Generation of CO and formate from eCO_2RR provides the OPs of -0.11 V and -0.20 V vs. RHE (pH=7)[32],

respectively. An increasing trend of absolute value of OPs can be observed with the sequence order for the CP-cell, GA-cell then GACP-cell. This means higher productions of CO and formate for both GA-cell and GAPC-cell which agrees well with our experimental results. However, the GA-cell shows a different profile for both results of CO_2 molar concentration and OP simulations, due to the unavailability of defining the exposure of graphene on GA in COMSOL® simulations.

To verify the stability for CP-cell and GACP-cell, we performed the eCO_2RR under -1.0 V vs. RHE in 1 M KOH with a constant CO_2 gas supply (15 mL min^{-1}). The durability test results for these cells are shown in **Figure 3**. The long-term experiment had been conducted for 4 hrs first and then paused to analysis the catholyte for liquid products. Then a new solution of 1 M KOH was added inside, and the reaction was continued for another 4 hrs. The tail gas was collected using a gas bag to analyse the gaseous products during each 4 hrs electrochemical test. From the reaction efficiency chronoamperometry (CA) diagram in Figure 3a and the FE results shown in Figure 3b, the FE values of CO are reduced from 63.28% to 22.93%, and the FE values of H_2 are increased from 34.92% to 75.53% at -1.0 V for the CP-cell. The FE values of CO are reduced from 83.36% to 79.27%, and FE value of H_2 increased from 5.74% to 12.50% at -1.0 V for the GACP-cell. It is found that the GACP-cell presents a better stability than the CP-cell, due to the homogenous distribution of CO_2 induced by porous bi-layer. Meanwhile, the catalyst layer is protected from peeling off from the carbon paper during the reaction, which leads to less carbon exposed to the electrolyte. GA also prevents the permeation of electrolyte through the gas diffusion layer (GDL) which leads the CP lost its GDE function.

The system's durability could also be influenced by the competing reaction of HER. After durability test, it is found the catholyte partially permeated through the CP GDE, which leads to a higher FE value for the CP-cell towards HER. GA's hydrophobic surface delays the liquid

penetration, which sustains a high FE value towards eCO_2RR. The catalyst morphology of GACP-cell before durability tests are characterised and shown in Figure 3c and Figure S6a, with the X-ray diffraction (XRD) results of Cu_2O coated CP in Figure S6b. The SEM image of electrode surface after durability test is illustrated in Figure 3d. Cu_2O nano cubes were found to uniformly distribute on the carbon paper before and after the durability test, which indicates that the structure of catalyst layer has not been destroyed without much loss of the catalyst loading. However, Cu_2O appears to be slightly corroded because of electrochemical corrosion, which could reduce its catalyst properties. This phenomenon could explain the decrease of FE value in the GACP-cell. Same catalyst corrosion is also observed on H-cell and CP-cell electrodes after durability test (**Figure S9**), this indicates that the catalysts degradation did not influence the gas diffusion layer discovery. Detailed data of durability test and relevant random error are listed in Table S9.

Further analysis on the pH influence on eCO_2RR performance is conducted by substituting electrolyte with 1 M $KHCO_3$. Same experimental condition and procedure were used, and testing were repeated for error proofing. Results are presented in **Figure S10** and Tables S10-15 show good agreement with above results and the same trend from 1 M KOH electrolyte. Again, the GACP-cell presents the highest FE of CO, which further proved the advances of the GA assisted porous bilayer electrode. While the FE of carbonaceous products is lower than that in 1 M KOH, due to the promoted HER in low pH conditions.

We then use the commercially available ATO nanoparticles as the eCO_2RR catalyst to investigate the feasibility of using GACP-cell to produce formate, which is in a liquid form. The performance of four types of cells are presented in **Figure 4**. Within the potential range of -0.4 V to -1.2 V vs. RHE, the H-cell (Figure 4a) presents the lowest FE values of formate and CO but the highest current density because the HER dominates the reaction. The CP-cell (Figure 4b) shows a

higher FE values towards eCO_2RR, and the GACP-cell obtained the highest FE values from all potentials. From the result, the FE values of formate in the CP-cell are 45.98%, 53.66%, 55.91%, 59.71%, 49.36% at a potential range from -0.4 V to -1.2 V, where FE values of formate in the GACP-cell (Figure 4d) are 70.10%, 76.91%, 78.11%, 82.98%, 84.54%, respectively. The full set of data for FEs and random errors are listed in Table S16-S21. For the GA-cell (Figure 4c), the exposed skeleton will only benefit water splitting and a lower FE value of eCO_2RR were obtained.

Figures 4e and 4f show the total current density and formate partial current density. The H-cell presents the highest current density towards HER, and the lowest current density of formate product. The other devices present similar current densities, and the GACP-cell shows the highest current density of formate. The results agree with our simulation results, as well as confirms the results from using Cu_2O catalyst.

In conclusion, we demonstrate to achieve a high FE of over 94% for CO and formate generation by improving the mass transfer of CO_2 reactant within the electrode. Results from the GACP-cell configuration shows the highest CO_2 molar concentration along the electrode surface. By using two types of catalysts, it has been confirmed that our GACP-cell can be applied for both gas and liquid systems. The influence of CO_2 supply is mainly due to device design which can enhance overall eCO_2RR performance and realise low cost and high efficiency eCO_2RR. This study also shed a light on improving eCO_2RR from engineering design point of view. By combining with advanced catalysts, a low energy consumption robust, industrialisation possible CO_2 to fuel conversion system could become a reality.

Experimental Section

Device Fabrication and Assembly: SOLIDWORKS® software was used for all electrochemical cell parts design. The drawings of all four type cells are presented in Figure S5 and Figure 1g. Formlabs® Form 2 3D printer with photopolymer resin (FLGPCL04) was used to print gas chamber, catholyte chamber and anode chamber. The inner size of two electrolyte chambers was 36 × 23 × 10 mm, and the injected electrolyte volume in each chamber was 7 mL. A small gap was designed above the chamber to avoid electrolyte spillage. For working electrode current supplying issue, conductive resin was used to connect carbon paper and titanium wire in H-cell. For CP-cell, GA-cell and GACP-cell, hollowed current collector plate and working electrode was compressed by hollowed compressing plate (area for middle gap: 2 cm^2).

Two materials were applied as the GDL. Carbon paper (CP, product code H23C6) was purchased from Freudenberg Ltd. Graphene aerogel was prepared based on the procedures reported in our pervious published work[27]. The CP and GA was cut into 18 × 21 mm^2 as the working electrode. For GACP-cell, the GA and CP were compressed and assembled in device. Detailed preparation process for the GDE followed the same route for all the cells, and the catalysts were coated on CP using hand brush and using spray gun for GA. The catalysts on GDEs as well as the cross section of the electrodes were characterised using XRD and scanning electron microscopy combined with energy-dispersive spectroscopy (SEM/EDS).

Electrochemical evaluation methods: All electrochemical results were recorded using potentiostat/ galvanostat (Metrohm Autolab® PGSTAT204). Reference electrode which converted to RHE using equation:

$$E_{RHE} = E_{Ag/AgCl} + 0.197\,V + 0.0591\,V \times pH \quad (2)$$

To evaluate the catalysis electrochemical performance for CO_2 reduction reaction, we performed electrochemical tests using different cells, and 1 M KOH and 5 M KOH were employed as catholyte and anolyte, respectively. The H-cell was purged with CO_2 (BOC 99.99%) for 30 min before the electrochemical tests and the pH of catholyte was measured as 13.8 after bubbling. For all the other GDE cells, pre-purge CO_2 into electrolyte is not necessary. The CO_2 gas flow rate during testing was controlled using a flow meter (Cole-Parmer TMR1-010462) with a value of 15 mL min^{-1}.

To analyse eCO_2RR behaviour in different cells, we performed the CA tests (Metrohm Autolab® PGSTAT128N potentiostat/ galvanostat) at -0.4 V, -0.6 V, -0.8 V, -1.0 V and -1.2 V vs. RHE for 1000 s. The current density (*j*) was recorded and then the gas/liquid products were collected for composition analysis using gas chromatography (GC, Shimazu Tracera GC-2010) with Barrieer Discharge Ionzation (BID) detector and ion chromatography (IC, equipped with 'Metrohm 6.1005.200' column formic acid identification). FE value of each product was calculated according to Faraday's Law[4].

$$\mathrm{FE} = \frac{\alpha\,\mathrm{n}\,\mathrm{F}}{\mathrm{Q}} \quad (3)$$

where α is the number of electrons transferred for reactants (e.g., α=2 for reduction of CO_2 to $HCOO^-$), n is moles of the desired product, F is Faraday's constant (96,500 C mol^{-1}), and Q means the total passed charge.

Two sets of the cells were manufactured, all above mentioned experiments were performed three times with random error is shown in brackets in Table S3 to S7, S9 to S14 and S16 to S20,

which indicates sample standard deviation. The current density (j) value in Table S8, S15 and S21 are calculated using the equation below:

$$j_a = j_{total} \times FE_a \quad (4)$$

Where j_a is the current density of a specific product, and the FE_a is the Faradaic efficiency of this product. No experimental error is included in Table S8, S15 and S21 because it is calculated value.

Supporting Information

Supporting Information is available from the Wiley Online Library or from the author.

Acknowledgements

This work is supported by the UK Engineering Physics and Science Research Council (Grant No. EP/S032886/1, EP/P026435/1 and EP/N007921).

Received: ((will be filled in by the editorial staff))
Revised: ((will be filled in by the editorial staff))
Published online: ((will be filled in by the editorial staff))

Declaration of Interests

There are no conflicts to declare.

References

[1] M. Bui, C. S. Adjiman, A. Bardow, E. J. Anthony, A. Boston, S. Brown, P. S. Fennell, S. Fuss, A. Galindo, L. A. Hackett, J. P. Hallett, H. J. Herzog, G. Jackson, J. Kemper, S. Krevor, G. C. Maitland, M. Matuszewski, I. S. Metcalfe, C. Petit, G. Puxty, J. Reimer, D. M. Reiner, E. S. Rubin, S. A. Scott, N. Shah, B. Smit, J. P. M. Trusler, P. Webley, J. Wilcox, N. Mac Dowell, Energy & Environmental Science **2018**, 11, 1062; F. M. Baena-Moreno, M. Rodríguez-Galán, F. Vega, B. Alonso-Fariñas, L. F. Vilches Arenas, B. Navarrete, Energy Sources, Part A: Recovery, Utilization, and Environmental Effects **2018**, 41, 1403.

[2] S. Liang, N. Altaf, L. Huang, Y. Gao, Q. Wang, Journal of CO2 Utilization **2020**, 35, 90; Y. Wu, S. Cao, J. Hou, Z. Li, B. Zhang, P. Zhai, Y. Zhang, L. Sun, Advanced Energy Materials **2020**, 10, 2000588.

[3] J. Qiao, Y. Liu, F. Hong, J. Zhang, Chem Soc Rev **2014**, 43, 631.

[4] D. D. Zhu, J. L. Liu, S. Z. Qiao, Advanced materials **2016**, 28, 3423.

[5] D. Raciti, C. Wang, ACS Energy Letters **2018**, 3, 1545; T. B. Cao-Thang Dinh, Md Golam Kibria, Ali Seifitokaldani, Christine M. Gabardo, F. Pelayo García de Arquer, Amirreza Kiani, Jonathan P. Edwards, Phil De Luna, Oleksandr S. Bushuyev, Chengqin Zou, Rafael Quintero-Bermudez, Yuanjie Pang, David Sinton, Edward H. Sargent, Science **2018**, 360, 783; T.-T. Zhuang, Y. Pang, Z.-Q. Liang, Z. Wang, Y. Li, C.-S. Tan, J. Li, C. T. Dinh, P. De Luna, P.-L. Hsieh, T. Burdyny, H.-H. Li, M. Liu, Y. Wang, F. Li, A. Proppe, A. Johnston, D.-H. Nam, Z.-Y. Wu, Y.-R. Zheng, A. H. Ip, H. Tan, L.-J. Chen, S.-H. Yu, S. O. Kelley, D. Sinton, E. H. Sargent, Nature Catalysis **2018**, 1, 946; S. Sen, D. Liu, G. T. R. Palmore, ACS Catalysis **2014**, 4, 3091; Y. Liu, S. Chen, X. Quan, H. Yu, J Am Chem Soc **2015**, 137, 11631; G. Lu, H. Wang, Z. Bian, X. Liu, ScientificWorldJournal **2013**, 2013, 424617; A. J. Garza, A. T. Bell, M. Head-Gordon, ACS Catalysis **2018**, 8, 1490.

[6] C.-H. Huang, C.-S. Tan, Aerosol and Air Quality Research **2013**, 14, 480; X. Xiaoding, J. Moulijn, Energy & Fuels **1996**, 10, 305; C. M. Gabardo, C. P. O'Brien, J. P. Edwards, C. McCallum, Y. Xu, C.-T. Dinh, J. Li, E. H. Sargent, D. Sinton, Joule **2019**, 3, 2777.

[7] J. Durst, A. Rudnev, A. Dutta, Y. Fu, J. Herranz, V. Kaliginedi, A. Kuzume, A. A. Permyakova, Y. Paratcha, P. Broekmann, CHIMIA International Journal for Chemistry **2015**, 69, 769; T. Zheng, K. Jiang, N. Ta, Y. Hu, J. Zeng, J. Liu, H. Wang, Joule **2019**, 3, 265.

[8] S. Nitopi, E. Bertheussen, S. B. Scott, X. Liu, A. K. Engstfeld, S. Horch, B. Seger, I. E. Stephens, K. Chan, C. Hahn, Chemical reviews **2019**, 119, 7610; T. Hatsukade, K. P. Kuhl, E. R. Cave, D. N. Abram, T. F. Jaramillo, Phys Chem Chem Phys **2014**, 16, 13814.

[9] D. C. Grills, Y. Matsubara, Y. Kuwahara, S. R. Golisz, D. A. Kurtz, B. A. Mello, J Phys Chem Lett **2014**, 5, 2033; H. A. Hansen, J. B. Varley, A. A. Peterson, J. K. Norskov, J Phys Chem Lett **2013**, 4, 388.

[10] W. Zhang, Y. Hu, L. Ma, G. Zhu, Y. Wang, X. Xue, R. Chen, S. Yang, Z. Jin, Adv Sci (Weinh) **2018**, 5, 1700275.

[11] R. Francke, B. Schille, M. Roemelt, Chem Rev **2018**, 118, 4631.

[12] Y. Peng, T. Wu, L. Sun, J. M. V. Nsanzimana, A. C. Fisher, X. Wang, ACS Appl Mater Interfaces **2017**, 9, 32782.

[13] N. Nilius, H. Fedderwitz, B. Gross, C. Noguera, J. Goniakowski, Phys Chem Chem Phys **2016**, 18, 6729.

[14] Y. Fu, Y. Li, X. Zhang, Y. Liu, J. Qiao, J. Zhang, D. P. Wilkinson, Applied Energy **2016**, 175, 536.

[15] X. Chang, T. Wang, Z. J. Zhao, P. Yang, J. Greeley, R. Mu, G. Zhang, Z. Gong, Z. Luo, J. Chen, Y. Cui, G. A. Ozin, J. Gong, Angew Chem Int Ed Engl **2018**, 57, 15415; A. Engelbrecht, C. Uhlig, O. Stark, M. Hämmerle, G. Schmid, E. Magori, K. Wiesner-Fleischer, M. Fleischer, R. Moos, Journal of The Electrochemical Society **2018**, 165, J3059.
[16] S. Kaneco, K. Iiba, H. Katsumata, T. Suzuki, K. Ohta, Electrochimica Acta **2006**, 51, 4880.
[17] S. Park, J.-W. Lee, B. N. Popov, International Journal of Hydrogen Energy **2012**, 37, 5850.
[18] K. Ogura, H. Yano, T. Tanaka, Catalysis Today **2004**, 98, 515.
[19] H. Yang, Q. Lin, C. Zhang, X. Yu, Z. Cheng, G. Li, Q. Hu, X. Ren, Q. Zhang, J. Liu, C. He, Nat Commun **2020**, 11, 593.
[20] H. Xiang, S. Rasul, K. Scott, J. Portoles, P. Cumpson, E. H. Yu, Journal of CO2 Utilization **2019**, 30, 214.
[21] N. Wang, R. K. Miao, G. Lee, A. Vomiero, D. Sinton, A. H. Ip, H. Liang, E. H. Sargent, SmartMat.
[22] F. P. G. De Arquer, C.-T. Dinh, A. Ozden, J. Wicks, C. McCallum, A. R. Kirmani, D.-H. Nam, C. Gabardo, A. Seifitokaldani, X. Wang, Science **2020**, 367, 661.
[23] D. Kopljar, A. Inan, P. Vindayer, N. Wagner, E. Klemm, Journal of Applied Electrochemistry **2014**, 44, 1107.
[24] J. Song, H. Song, B. Kim, J. Oh, Catalysts **2019**, 9, 224.
[25] T. Burdyny, W. A. Smith, Energy & Environmental Science **2019**, 12, 1442.
[26] K. Junge Puring, D. Siegmund, J. Timm, F. Möllenbruck, S. Schemme, R. Marschall, U. P. Apfel, Advanced Sustainable Systems **2021**, 5, 2000088; S. Garg, M. Li, T. E. Rufford, L. Ge, V. Rudolph, R. Knibbe, M. Konarova, G. G. Wang, ChemSusChem **2020**, 13, 304.
[27] X. Liu, J. Xi, B. B. Xu, B. Fang, Y. Wang, M. Bayati, K. Scott, C. Gao, Small Methods **2018**, 2, 1800138.
[28] C. K. Ho, S. W. Webb, *Gas transport in porous media*, Vol. 20, Springer, **2006**.
[29] J. H. Montoya, C. Shi, K. Chan, J. K. Norskov, J Phys Chem Lett **2015**, 6, 2032; S. Popović, M. Smiljanić, P. Jovanovič, J. Vavra, R. Buonsanti, N. Hodnik, Angewandte Chemie International Edition **2020**, 59, 14736.
[30] Y. Chen, M. W. Kanan, J Am Chem Soc **2012**, 134, 1986; N. Han, P. Ding, L. He, Y. Li, Y. Li, Advanced Energy Materials **2020**, 10, 1902338; Y. Zhou, R. Zhou, X. Zhu, N. Han, B. Song, T. Liu, G. Hu, Y. Li, J. Lu, Y. Li, Advanced Materials **2020**, 32, 2000992; F. Li, M. Xue, J. Li, X. Ma, L. Chen, X. Zhang, D. R. MacFarlane, J. Zhang, Angewandte Chemie **2017**, 129, 14910.
[31] J. Resasco, L. D. Chen, E. Clark, C. Tsai, C. Hahn, T. F. Jaramillo, K. Chan, A. T. Bell, J Am Chem Soc **2017**, 139, 11277.
[32] J. Wu, Y. Huang, W. Ye, Y. Li, Adv Sci (Weinh) **2017**, 4, 1700194.

Figure 1 Schematic illustrations of design for a) CP-electrode, b) GACP-electrode; integrated design for c) CP-cell and d) GACP-cell, components arrangement from left to right are gas chamber (white: gas channel for CP-cell, black: GA for GACP-cell, respectively), catalyst coated carbon paper (brown), reference electrode (blue) in catholyte, ion exchange membrane (light blue), counter electrode (yellow) in anolyte; e) cross-section view of bilayer with catalyst layer and GA (insertion); f) CO_2 mass transfer pathway, CO_2 transfer through GA (black), CP (grey) and catalyst layer (yellow); fabrication of GACP-cell with g) multi-components, h) top view of bilayer with coated catalyst, i) disassembled and j) assembled cells.

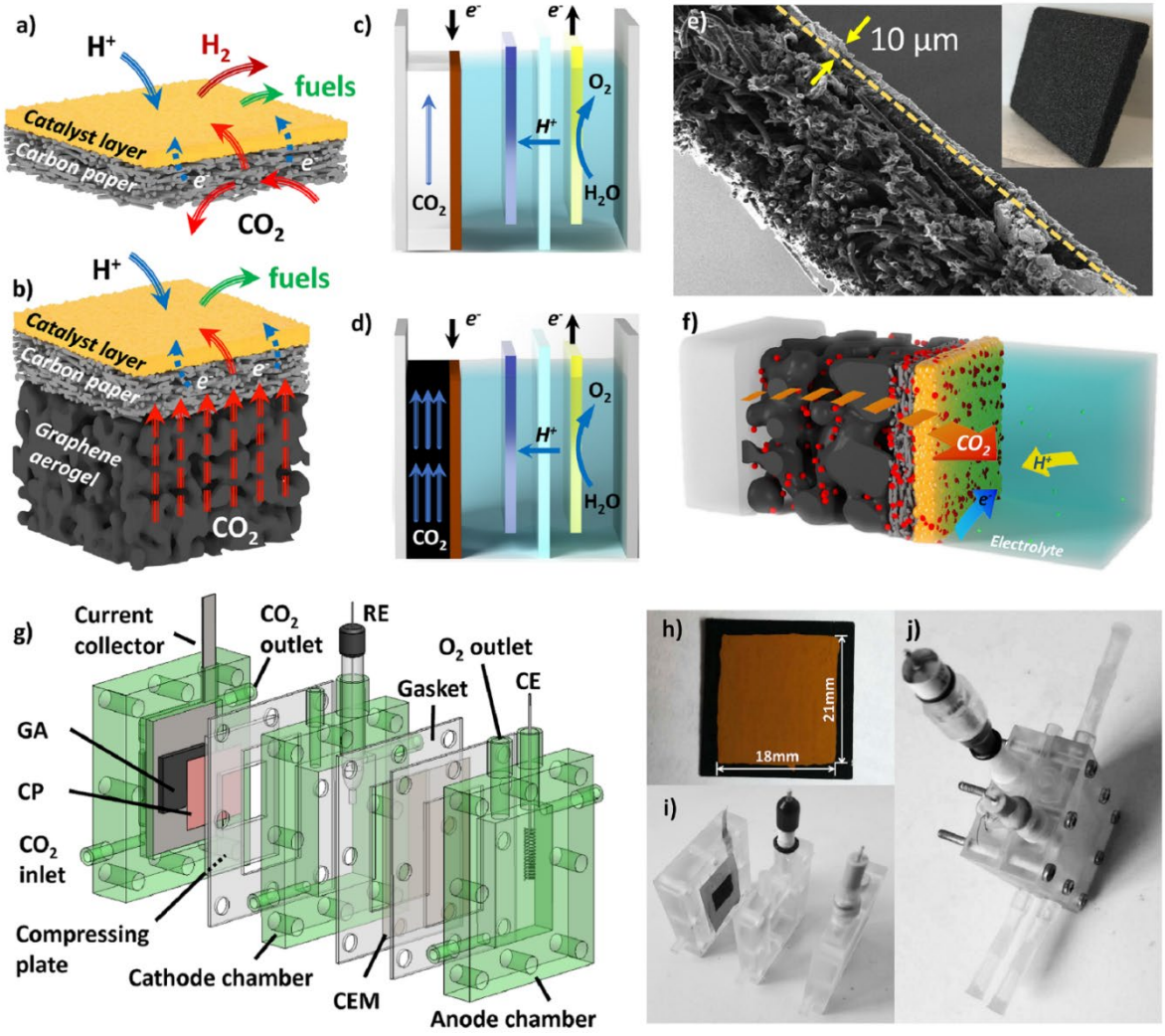

Figure 2 COMSOL® simulation on CO_2 molar concentration along the cathode catalyst layer for a) CP-cell b) GA-cell and c) GACP-cell; Faradaic efficiency profiles of d) CP-cell, e) GA-cell, f) GACP-cell and g) H-cell using Cu_2O catalyst in 1 M KOH electrolyte of eCO_2RR with products including CO (yellow, bottom), Formate (blue, middle), H_2 (green, top); e) Total current density for results in d-g). f) Current density of CO for results in d-g).

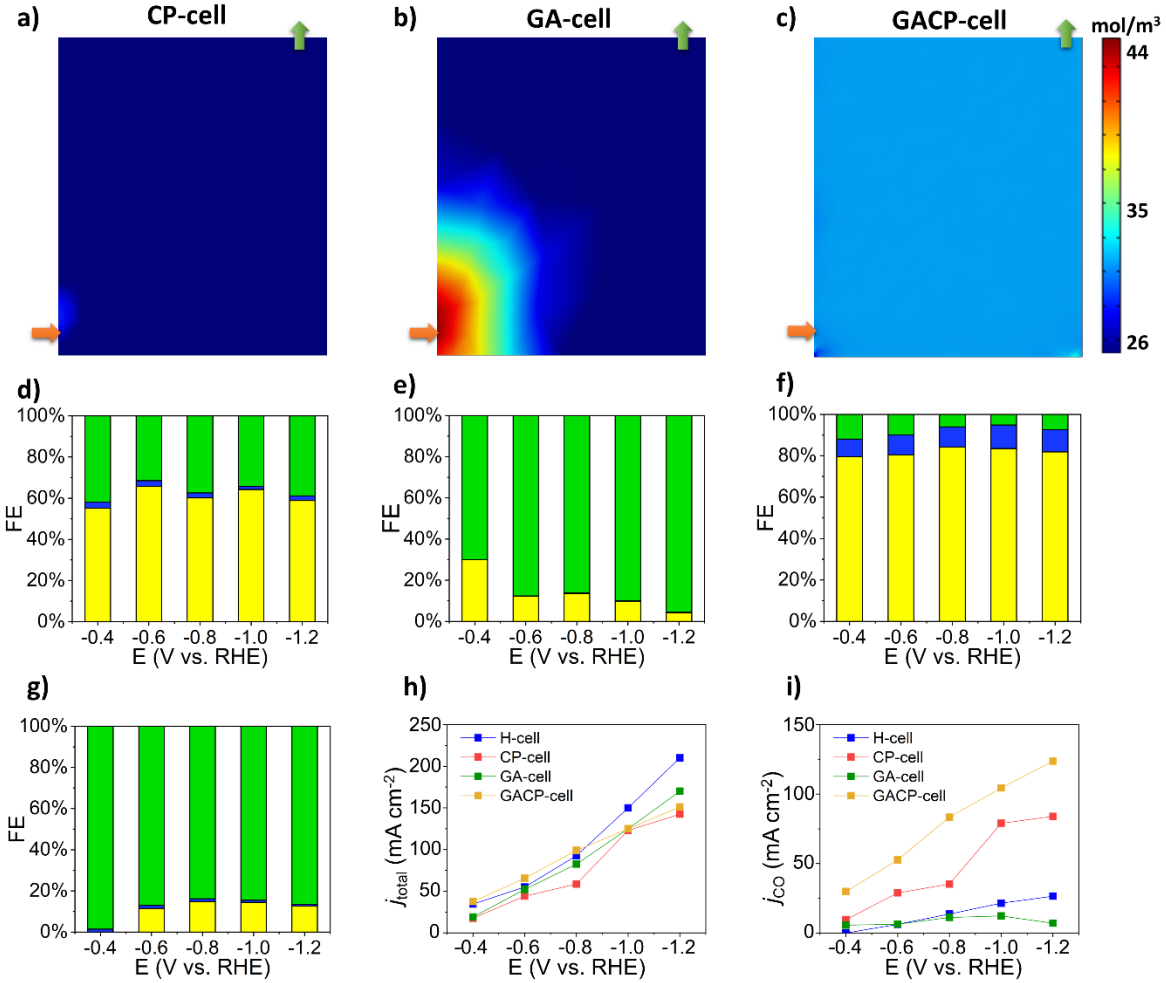

Figure 3 Durability test results under 1 V vs. RHE of CP-cell and GACP-cell a) Chrono amperometry plot b) FE graph for CP and CPGA cell at 4th and 8th hours for durability test, c) and d) SEM of the catalyst surface of GACP-cell before and after durability test.

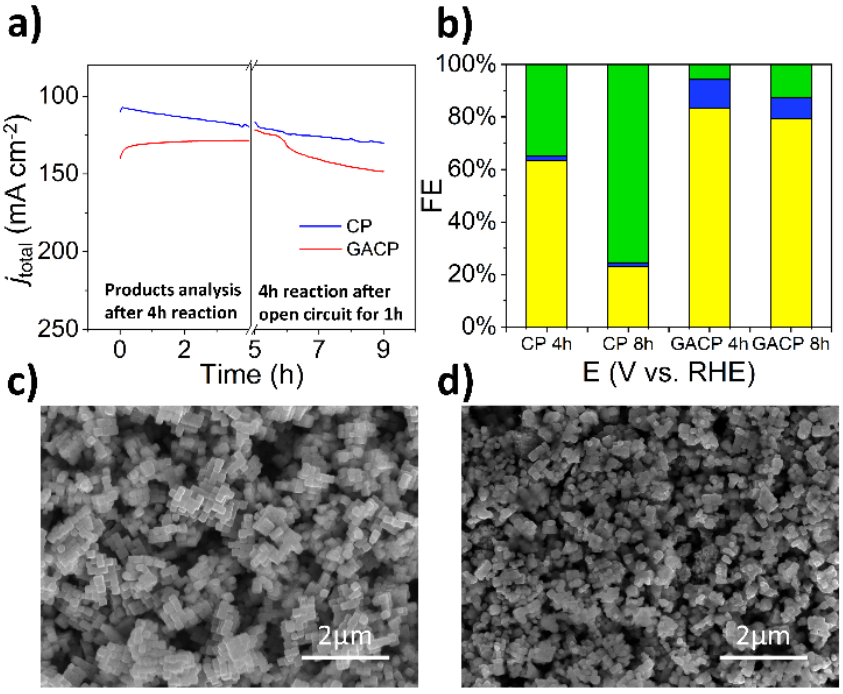

Figure 4 Faradaic efficiency profiles of a) H-cell b) CP-cell c) GA-cell d) GACP-cell using ATO catalyst in 1 M KOH electrolyte of eCO_2RR with products including formate (blue, bottom), H_2 (green, top) and CO (yellow, middle). e) Total Current density for results a-d), f) Current density of formate for results a-d)